In: New Developments in Condensed Matter Physics
Editor: John V. Chang, pp. 103-128
ISBN: 1-59454-822-6
© 2006 Nova Science Publishers, Inc.

Chapter 5

OPTICAL PROPERTIES OF NANOCRYSTALLINE ZNO THIN FILMS GROWN USING PULSED LASER DEPOSITION

E. McGlynn[1*], J. Fryar[1], G. Tobin[1], C. Roy[1✠], S. Byrne[1], J.-P. Mosnier[1], E. de Posada[2], D. O'Mahony[2], J.G. Lunney[2], M.O. Henry[1]

[1]School of Physical Sciences / National Centre for Plasma Science & Technology, Dublin City University, Glasnevin, Dublin 9, Ireland.

[2] Physics Department, Trinity College Dublin, Dublin 2, Ireland.

Abstract

Raman spectroscopy, x-ray diffractometry, atomic force microscopy, photoluminescence spectroscopy and reflectance spectroscopy have been used to characterize ZnO thin films grown by pulsed laser deposition as a function of the post-growth annealing temperature.

Raman results show enhancement and broadening of certain Raman features which correlate with changes in the widths of the x-ray diffraction peaks for samples with varying grain size in the 50-100 nm range. These data suggest that electric fields, arising from charge trapping at grain boundaries, in conjunction with localised and surface phonon modes, are the cause of the intensity enhancement and asymmetry of the Raman features.

Band-edge photoluminescence and reflectance spectra also altered considerably with increases in grain size, showing clearly observable excitonic structure in the reflectance spectra. An analysis using a deformation potential Hamiltonian demonstrates that the experimental exciton energies are not explicable solely in terms of sample strain and give additional evidence for electric fields in the samples due to charge trapping at grain boundaries. This is supported by theoretical estimates of the exciton energy perturbation due to electric fields and also by the behaviour of the green band in the samples.

Detailed studies show that reflectance spectra in nanocrystalline ZnO differ substantially from bulk material. Interaction of excitons, damped by strong electric field effects, with photons leads to exciton-polaritons with substantial damping, eliminating the normal Fabry-

* E-mail address: enda.mcglynn@dcu.ie
✠ Deceased

Perot structure seen in thin films. Good qualitative agreement is achieved between the model and data and the conclusions are also in good agreement with the photoluminescence and Raman data.

Finally, high intensity optical pumping data of these samples again shows a dependence on grain size. All samples show evidence of high excitation effects and the sample with the largest grain size displays random lasing at room temperature.

All our results indicate the very strong influence of electric fields due to charge trapping at grain boundaries on the optical properties of nanocrystalline ZnO.

Keywords: ZnO, thin films, photoluminescence, x-ray diffraction, Raman spectroscopy, exciton, stimulated emission.

Introduction

ZnO has recently become the topic of intense renewed research due to its potential use in short wavelength light emitters such as LEDs and laser diodes. ZnO is a semiconducting oxide with a direct bandgap of approxmimately 3.3 eV at room temperature. ZnO has a number of exceptional material properties which give it great potential as a materials system for efficient wide bandgap devices. These properties include a large (~ 60 meV) exciton binding energy, leading to efficient excitonic emission at room temperature, the availability of high quality, large area single crystal ZnO substrates for homoepitaxy and good radiation hardness [1-3]. In addition, the main technological challenge of achieving p-type doping with sufficiently high carrier concentrations and mobilities is beginning to be conquered now, through a variety of approaches involving various dopants and methods [4-6]. Furthermore, ZnO shows exceptional promise as a material for nano-optoelectronics and electronics, as a wide range of nanostructures such as nanorods, belts, quantum dots and other morphologies can be grown in a controllable manner and with a degree of self organization [7-9].

One of the main challenges in the achievement of the technological goals for ZnO and its alloys is to fully understand the materials science involved in the growth of high quality thin films. Given that a large literature on the optical and electronic properties of bulk ZnO exists since the 1950's and before [10], the utilization and transfer of such knowledge and data to thin film growth and characterization is a key area of research. ZnO thin films have been successfully grown by a variety of techniques such as pulsed laser deposition (PLD), metallo-organic vapour phase epitaxy (MOVPE), molecular beam epitaxy (MBE), magnetron sputtering and others. Among these techniques, PLD has been consistently shown to grow films of the highest quality and is excellently suited to this material system [11-14].

In this paper, we give a full report of the results of a study of a number of ZnO thin films grown using PLD, with various post-growth anneals which led to a variety of grain sizes. We examine the systematic behaviour shown by these samples using Raman spectroscopy (RS), x-ray diffraction (XRD), atomic force microscopy (AFM) and both photoluminesence (PL) and reflectance spectroscopies

Experimental Details

ZnO films were grown on (0001) sapphire substrates by PLD using a 10 Hz pulsed KrF excimer laser (with wavelength λ=248 nm). The fluence on target was fixed at 1.7 J/cm^2 for all samples. A ZnO ceramic target (99.99%) was used throughout and the target to substrate distance was ~ 4 cm. The thin films were grown in an O_2 (purity 99.99%) pressure of 0.3 mbar and the substrate temperature was maintained at 400°C during growth. The film thicknesses were in the range 150-200 nm, giving a deposition rate of 0.025 nm/pulse. Two of the films were subsequently annealed in O_2 (0.3 mbar) at 400°C and 500°C respectively (see table 1) in the growth chamber immediately after deposition. SEM data show that the films are continuous and show no evidence of porosity. The crystal structure and quality of the samples were investigated by XRD in the θ-2θ mode and also in phi scan mode (using Cu K_α radiation). Raman scattering measurements were performed using a micro-Raman spectrometer equipped with a CCD detector. Raman spectra were excited with 1.96 eV photons from a He-Ne laser (λ~632 nm) or, for the resonance excitation measurements, with 3.82 eV photons from a UV laser (λ=325 nm), in both cases using unpolarised back scattering geometry. The He-Ne laser beam of 5-6 mW was focussed on the sample surface to a spot of diameter ~ 10 μm. Atomic force microscopy (AFM) measurements were made using a commercial AFM in contact mode operation. The 325 nm line of a continuous wave HeCd laser (output ~ 40 mW unfocussed on the sample) provided PL excitation. The PL emission from the sample was analyzed using a 1 metre grating spectrometer and detected with a photomultiplier tube operated in photon counting mode. Controllable temperatures from 10 K to 300 K were achieved using a closed cycle cryostat. Reflectance measurements were performed using a Fourier-transform (FT) spectrometer fitted with a photomultiplier tube. Samples were studied at temperatures between 20 and 300 K using a closed-cycle cryostat. A 150 W Xe-arc lamp was used to illuminate the samples after beam confinement through a variable aperture. No focusing was used and the incident light was unpolarised. Since the spectral region of interest is in the UV, and to avoid saturation of the detector (due to the multiplex nature of the FT spectrometer data acquisition), visible wavelengths were removed from the reflected beam with an appropriate glass filter. As a reference, we used a silicon sample onto which a thick layer of aluminium was deposited. Typical reflectivity for this reference sample is approximately 93 %. High-intensity optical pumping is by the frequency-tripled output (355nm) of a Nd:YAG laser (10Hz, 6ns). The pump power intensity was lowered using reflection from a glass slide and a neutral density filter. The laser spot was focused onto the sample with a diameter of 1.2mm, thus we achieved excitation intensities in the range 500 - 7000 kW/cm^2. The laser strikes the sample at normal incidence. The edge emission from the sample was analysed using the grating spectrometer system described above. The typical spectral resolution of the PL and reflectance data was in the range 0.25 meV to 0.1 meV for bandedge PL and reflectance studies and 1 meV or greater for the data measured across a broader spectral range.

Table 1: Growth conditions and results of x-ray analysis for PLD-grown ZnO thin films.

Sample	Annealing temp. (^{o}C)	Annealing time (min)	FWHM of (0002) peak (^{o})	Average grain size (nm)
(i)	No anneal	-	0.34	32
(ii)	400	10	0.22	67
(iii)	500	15	0.21	79

Results

X-ray diffraction measurements in the θ-2θ mode as a function of sample annealing temperature are presented in figure 1(a). They are dominated by the (0002) and (0004) ZnO peaks along with the prominent (0006) sapphire peak in the annealed samples. The sapphire peak is not seen for sample (i), possibly due to increased surface scattering due to surface roughness in this case. The surface roughnesses (taken as the standard deviation of the AFM tip height across a 2 μm profile) vary from > 10 nm for sample (i) down to ~3 nm for sample (iii). The dominance of the (0002) and (0004) peaks indicates that ZnO thin films highly textured along the (0001) direction have been grown [15]. Figure 1(b) shows the phi scan of the PLD sample annealed at 500^{0}C for the ZnO $(10\bar{1}1)$ planes and the sapphire $(10\bar{1}4)$ planes. The presence of peaks in the ZnO phi scans separated by 60^{0} confirms the in-plane epitaxial ordering for all these samples and the angular displacement (30^{0}) of the ZnO and sapphire peaks confirms the epitaxial relationship between ZnO and sapphire as $[0001]_{ZnO}$ // $[0001]_{Sapphire}$ perpendicular to the substrate and $[10\bar{1}0]_{ZnO}$ // $[21\bar{3}0]_{Sapphire}$ in the plane of the substrate. Similar phi scans were obtained for the other PLD samples, with the same epitaxial relationship in evidence. There was evidence of an additional epitaxial orientation in the sample annealed at 400^{0}C, however the relative magnitude of this second orientation was rather small compared to the dominant orientation. The lattice parameters of the ZnO thin films perpendicular to the substrate can be calculated from the diffraction angles in the θ-2θ mode corresponding to the $(10\bar{1}0)$ and (0002) planes. The intensity of the $10\bar{1}0$ peak is small compared to the (0002) peak intensity due to the high degree of c-axis orientation. The average values of c- and a-axis lattice constants of our PLD samples are 0.518 nm and 0.330 nm respectively and the values for all samples were identical within the limits of our experimental accuracy (± 0.001 nm). The average grain size (parallel to the (0002) direction) of the ZnO films can be estimated from the full width at half maximum (FWHM) of the (0002) peak using Scherrer's relation [16] (see table 1). The range of annealing temperatures used in our work coincides with those known to lead to major grain growth [17-18]. The annealed samples show a decrease of (0002) peak FWHM and consequent increase in grain size with increasing annealing temperature. These results are supported by AFM imaging of the samples (figure 2), where measurements of the lateral grain sizes are 135 ± 40 nm for the sample annealed at 400^{0}C and 180 ± 50 nm for the sample annealed at 500^{0}C. The annealing process clearly produces a recovery of the crystal structure and increase of the grain size. We note that in our experimental conditions, the increase in grain size is achieved after annealing for relatively short times. Such an effect was also observed in the case of magnetron sputtered ZnO [19].

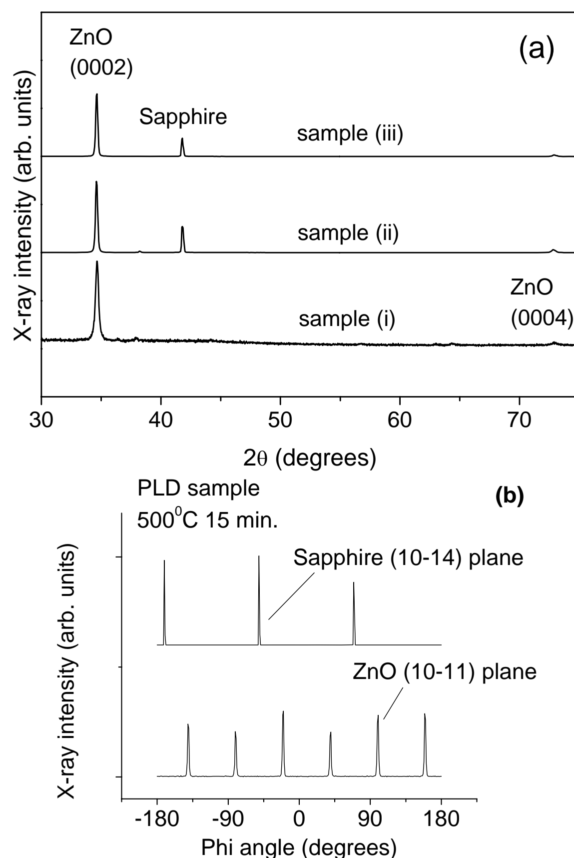

Figure 1: (a) θ-2θ XRD scans showing the (0002) and (0004) Bragg peaks obtained from the PLD-grown ZnO films : (i) unannealed; (ii) and (iii) annealed at 400°C and 500°C respectively. (b) XRD phi scan of the PLD sample annealed at 500°C for the ZnO ($10\bar{1}1$) plane and the sapphire ($10\bar{1}4$) plane.

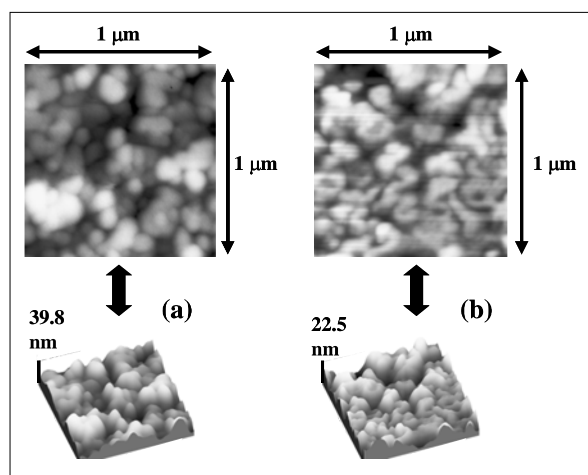

Figure 2: AFM images of PLD-grown ZnO thin films: (a) annealed at 400^0C; (b) annealed at 500^0C. The average grain sizes estimated from these images are 135 ± 40 nm for the sample annealed at 400^0C and 180 ± 50 nm for the sample annealed at 500^0C.

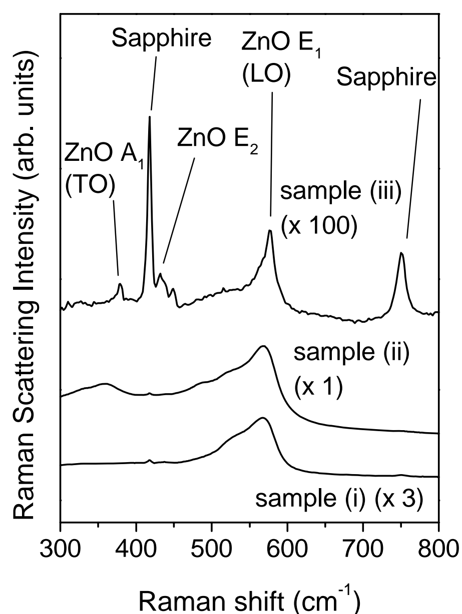

Figure 3: Non-resonant (λ_{exc} = 632 nm) Raman spectra of PLD grown ZnO thin films : (i) not annealed; (ii) and (iii) annealed at 400°C and 500°C respectively.

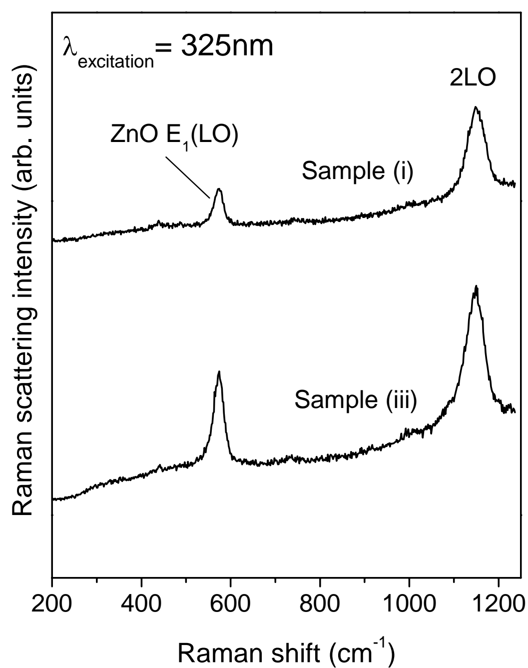

Figure 4: Resonant (λ_{exc} = 325 nm) Raman spectra of PLD grown ZnO thin films : (i) not annealed and (iii) annealed at 500°C. Similar spectra were obtained for the other samples. The 2LO feature characteristic of resonant Raman spectra is clearly seen at ~ 1150 cm^{-1}.

The unpolarized Raman spectra (with He-Ne excitation) of the ZnO thin films are shown in figure 3 as a function of annealing temperature. The peaks at 418 cm^{-1} and 751 cm^{-1} are due to scattering from the sapphire substrate. The E_2 437cm^{-1} peak, characteristic of the wurtzite lattice, can be seen in all samples. The A_1(TO) mode at 379 cm^{-1} is apparent in sample c. However, the Raman spectra are dominated by the longitudinal optical vibration at ~570cm^{-1}. This band is attributed to the E_1(LO) mode [20]. The intensity and FWHM of the 570 cm^{-1} peak appears anomalously high for the unannealed sample and the sample (ii) which was annealed at 400^{0}C, but it is reduced dramatically (by a factor of ~100 relative to the sapphire features) with increasing annealing temperature. In addition, this feature shows a marked asymmetry which also decreases with increasing annealing temperature. Raman spectra were also measured with UV excitation λ=325 nm (or 3.82eV) and are shown in figure 4. The spectra from all the samples are similar, that is the strong band at 570 cm^{-1} was observed below the 800 cm^{-1} spectral region whereas a 2LO vibrational mode at ~1150 cm^{-1} was recorded in the higher spectral range as reported by several authors [21-22]. The Raman peak at 570 cm^{-1} is symmetric for all the PLD-grown ZnO samples when the excitation is at or above resonance.

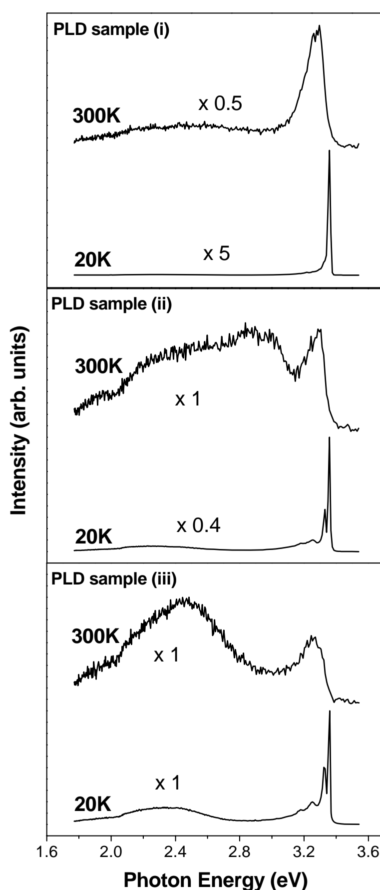

Figure 5: PL data for the three PLD samples at 20 K and 300 K. Multipliers given allow comparison of the three sample intensities at the same temperature, but do not relate the 300 K measurements to the 20 K measurements.

Figure 5 shows PL spectra at 20 K and 300 K for the three PLD grown samples. These spectra show that all the samples have strong band-edge, UV emission and with varying amounts of green band emission. Other workers have found similar results for ZnO materials grown using PLD [23]. The low temperature bound exciton (BE) luminescence in the case of the PLD samples is substantially broadened, and the multiple sharp BE lines seen in the bulk material cannot be resolved in our PLD material. The width of the BE feature in PLD material at 20K is ~12 meV compared to the bulk crystal value for a single line of ~1 meV. We note that the room temperature peak PL intensities for all three samples are quite similar, with the unannealed sample actually having the highest peak intensity. The room temperature integrated intensities across the entire spectral range of the annealed samples are slightly higher than that of the unannealed samples. At low temperatures however, we see that the peak and integrated intensity of the unannealed sample is substantially lower than the annealed samples. The integrated intensities of the two annealed samples are quite similar at low temperature. One must be careful in making sample to sample comparisons of PL intensities due to the variations that may occur in alignment etc., however there is a very definite increase in low temperature PL intensity from the unannealed sample to the two annealed samples. We also note a relative increase in the intensity of the green band (~ 2.4 eV) compared to the band-edge emission with increased annealing, and the appearance of a structured luminescence below the BE emission in the two annealed samples which is not present in the unannealed sample.

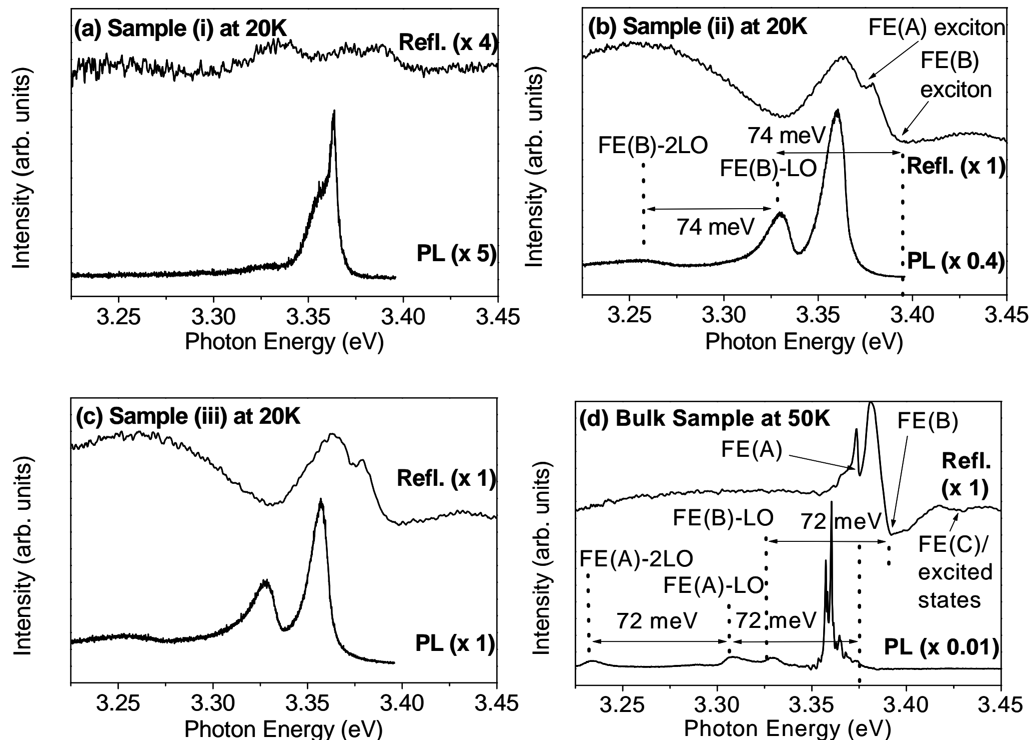

Figure 6: PL and reflectance (at 45^0 incidence angle) data for the three PLD samples at 20 K and the bulk material at 50 K. Positions of FE and LO phonon replicas are indicated for sample (ii) and the bulk crystal, with similar assignments for samples (i) and (iii). All linewidths are sample limited.

In figure 6 we compare PL and reflectance (at 45^0 incidence angle) data for the three PLD grown samples at 20 K and for the bulk crystal at 50 K (temperature for the bulk sample was chosen to show LO phonons replicas more strongly) in the near band-edge region of the spectrum. For all samples, as noted above, we see BE luminescence in the region around 3.360 eV. In the bulk crystal we observe longitudinal optic (LO) phonon replicas of both the A and B free excitons (FE), with some evidence (from the PL temperature dependance) of zero-phonon luminescence from the A exciton above the BE lines.

Figure 7 shows the more detailed experimental reflectance data (at normal incidence to simplify subsequent modelling, which accounts for minor differences in structure compared to figure 6) for the PLD samples at 17 K. In the top curve of figure 7 the excitonic features are only weakly observable, and some evidence is seen of oscillatory structure at higher and lower energies. The A- and B-exciton features (region II) are much clearer in the two annealed samples, the middle and lower curves of figure 7, and also show clear oscillations at both low and high energies (regions I and III). We believe, on the basis of the analysis below, that these oscillations are Fabry-Perot (FP) oscillations due to multiple reflections in the thin film. In our samples no evidence is seen of the short period oscillations characteristic of anomalous wave interference. Figure 8 shows a comparison of the reflectance spectra of the PLD sample annealed at 500^0C (bottom curve) and a single crystal ZnO sample (middle curve) at 20 K. For the bulk single crystal reflectance anomalies corresponding to the A- and B-excitons are seen at ~3.374 eV and ~3.390 eV respectively. We also see evidence of the excitonic excited states at ~3.427 eV but will neglect the contribution of these states in the subsequent analysis [24-25]. No evidence of the excited states are seen in any of the PLD samples. The bulk sample shows no evidence of the FP oscillations in regions I and III. The excitonic features in region II are substantially quenched for the PLD sample in comparison to the bulk.

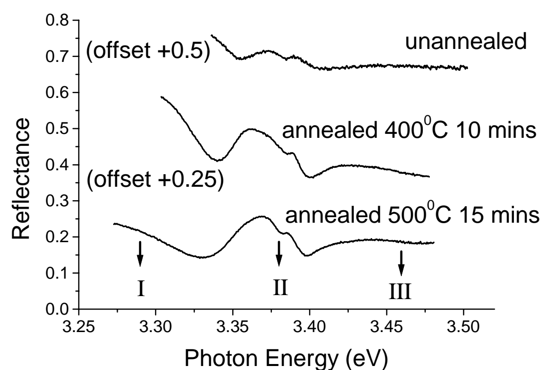

Figure 7: Experimental reflectance data (at normal incidence) for PLD samples at 17 K: unannealed, annealed at 400^0C for 10 minutes and annealed at 500^0C for 15 minutes.

High intensity optical pumping is done by the frequency-tripled output of a Nd:YAG laser as mentioned above. Figure 9 shows the variation of the luminescence spectra for the bulk crystal sample with varying pump power. We see two features that dominate the spectra, firstly at higher photon energies we believe to be the free exciton at 380nm (based on comparison with spectra taken with HeCd excitation) and a band centred at 405nm, with a separation of ~150meV from the free exciton, due to the exciton-electron interaction (n-type

concentration in these samples ~ $10^{17}cm^{-3}$) [26]. A plot of integrated emission intensity versus excitation reveals linear behaviour with no threshold and no evidence of coherent emission or a speckle-like appearance was seen for this sample. We see no evidence of the P-band or electron-hole pair (EHP) emission normally associated with the high pumping regime in ZnO [26-27].

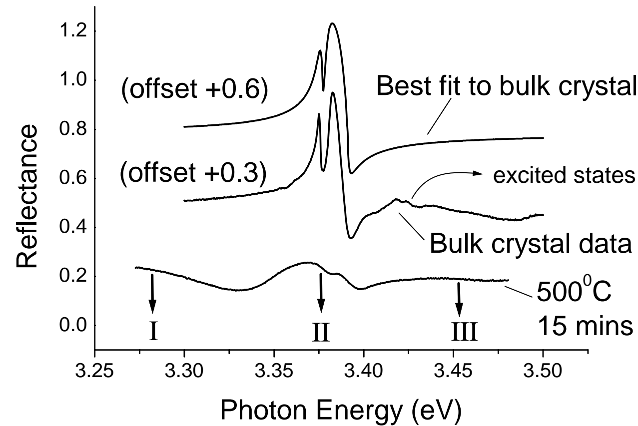

Figure 8: Comparison of the normal incidence reflectance spectra (at 17 K) of the PLD sample annealed at 500^0C (bottom curve) and a single crystal bulk ZnO sample (at 20 K) (middle curve). The top curve shows the best fit to the experimental data for the bulk crystal using the model described in the text.

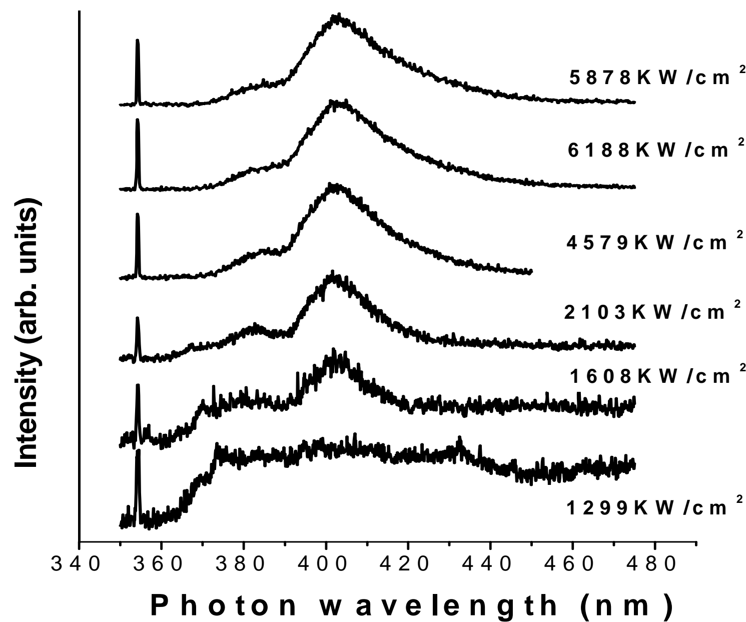

Figure 9: Bulk material emission spectra at room temperature excited by 355nm line at various power densities.

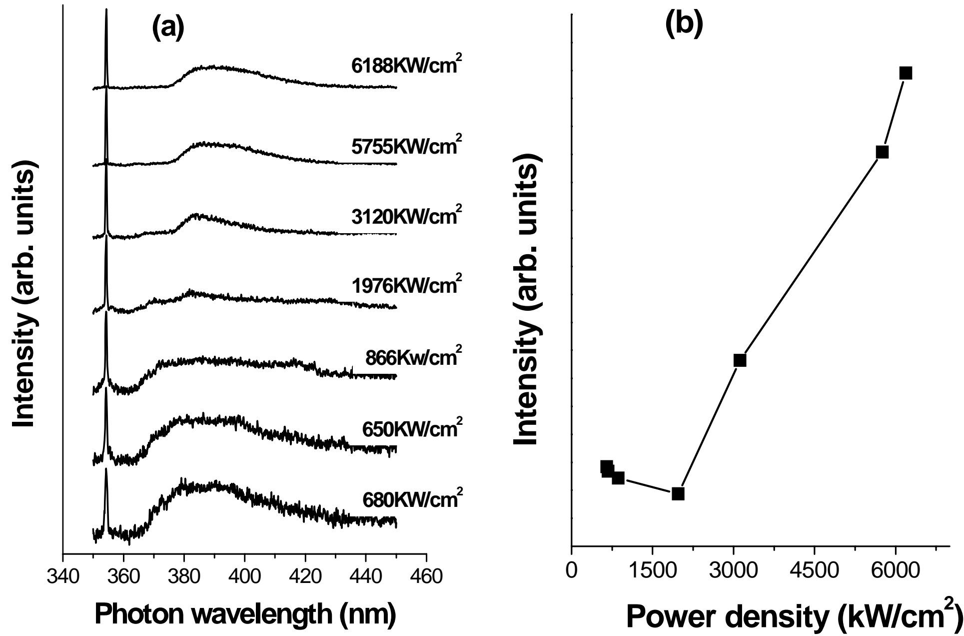

Figure 10: (a) sample (i), emission spectra at room temperature excited by 355nm line at various power densities; (b) the room temperature dependency of integrated output intensity versus excitation intensity.

If we now examine the PLD grown samples, looking at sample (i) in figure 10(a), we see a rather broad band, which at low excitation intensities is centred at ~382 nm, close to the expected free exciton energy. At higher excitations we begin to see a band appearing at the low energy side of the free exciton. This is really observed simply as an increase in the asymmetry to lower energies of the band and thus it is hard to associate a central energy to this emerging band. However we believe that we are seeing the emergence of the P-band, associated with exciton-exciton collisions, associated with the high pumping regime in ZnO. This band would be expected in the range 80 – 100 meV below the free exciton, corresponding to a wavelength of ~393 nm. The P band, where an exciton-exciton collision gives rise to an emitted photon and an exciton excited into a higher state will have a range of energies given by [26-27]

$$P_n = E_{ex} - E_b^{ex}\left(1 - \frac{1}{n^2}\right) - \frac{3}{2}kT \quad (n = 2,3,4,\ldots,\infty), \qquad (1)$$

where P_n is the photon energy, E_{ex} the free-exciton emission energy, $E^{ex}{}_b$ the binding energy of the exciton, n the quantum number of the envelope function, and KT is the thermal energy. Equation (1) gives 83 meV for n = 2 and ~98 meV for infinite n, as the energy difference between the free exciton peak and the exciton-exciton peak. Thus in PLD samples with relatively broad excitonic features we expect to see a P-band in the range 80–100 meV below the free exciton energy. Figure 10(b) also shows the integrated intensity as a function of the excitation intensity. There is a steep increase in the curve at approximately 2000 kW/cm^2.

Thus we see the onset of high excitation effects with the appearance of the P-band and a nonlinear dependence of intensity with excitation level. For sample (ii), shown in figure 11, we again see rather similar spectra, with a free exciton band centred at ~ 380 nm, and the appearance of a band at lower energies with increasing excitation levels, which we again associate with the P-band. For sample (iii) shown in figure 12 (a), we see a broad free exciton feature at 387nm. The slight shift to lower energies is attributed to the sample annealing, leading to a reduction in grain-boundary electric fields, which lowers the free exciton energy slightly. At intensities above 2253 kW/cm^2, we observe a relatively sharp feature at 397nm, which is only visible at high excitation energies (marked with the arrows in figure 12 (a)). Visually, above this threshold of ~ 2000 kW/cm^2, one can see a violet speckled appearance on the sample surface, not seen at lower excitations or with HeCd excitation. This effect is also visible in a plot of the integrated luminescence versus excitation density (figure 12 (b)), which shows a clear threshold at slightly greater than 2253 kW/cm^2. In addition to the high excitation effects seen for other samples, this sample clearly shows evidence for lasing in random media. The peak occurs quite identifiably in the P-band range and above threshold we see both an increase and narrowing of the spectral feature, expected during the lasing process. We see evidence of mode structure, but the pulse to pulse variability of this structure due to the random lasing process means that it varies from spectrum to spectrum [27-28].

The evolution of the stimulated emission as a function of the sample treatment shows that sample (iii) has the strongest signals in the P-band, and is the only sample to show lasing, although high excitation effects are seen in all samples and the thresholds at which high excitation effects are seen between the various samples appear relatively constant at ~2000 kW/cm^2. Sample (iii) has a grain size of ~ 80 nm (table 1) and there is a relatively large difference in the grain sizes between the unannealed and annealed samples.

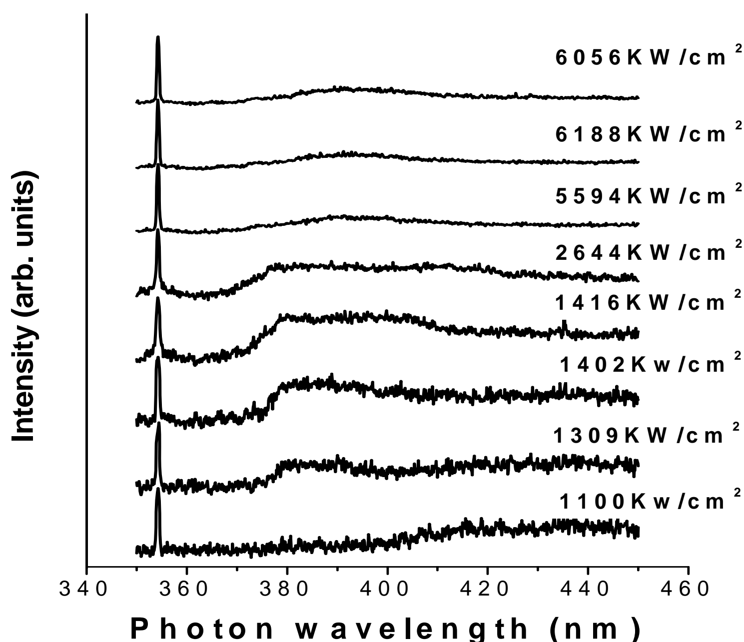

Figure 11: Sample (ii) emission spectra at room temperature excited by 355nm line at various power densities.

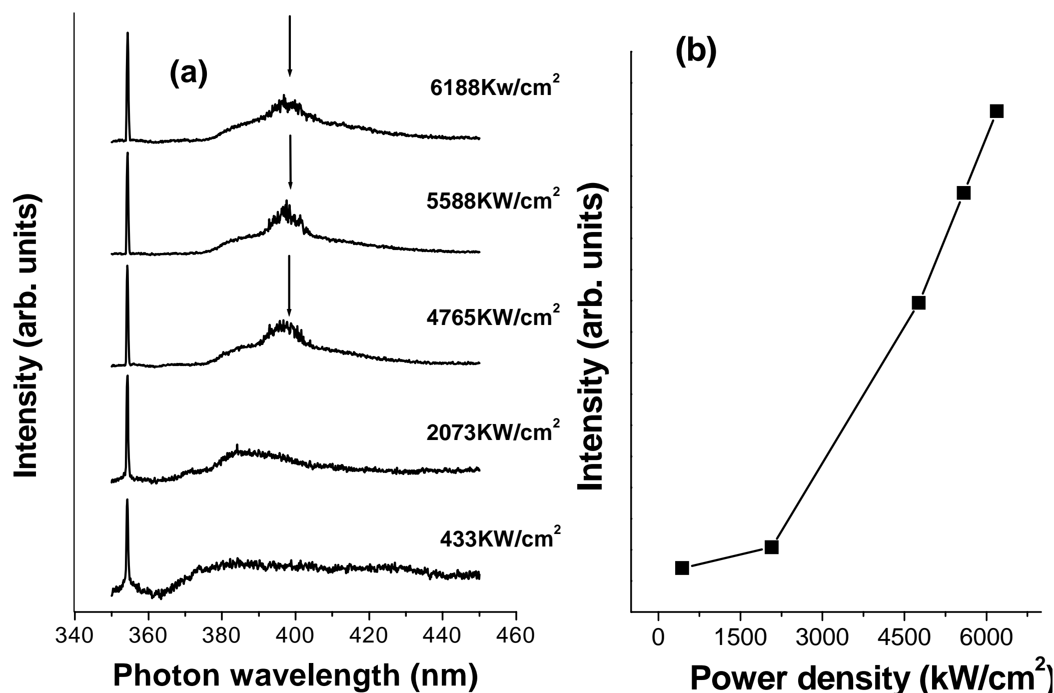

Figure 12: (a) sample (iii), emission spectra at room temperature excited by 355nm line at various power densities; (b) the room temperature dependency of integrated output intensity versus excitation intensity.

Discussion

We observe a clear correlation between the XRD data and the corresponding non-resonant Raman spectra as a function of annealing temperature. As the average grain size increases, we observe a reduction in the relative intensity and asymmetry of the 570 cm^{-1} band in the Raman spectra. The origin of the intensity enhancement and asymmetry of the LO mode at 570cm^{-1} in nanocrystalline ZnO has been widely discussed in the literature. Explanations for this structure include resonance enhancement due to impurity levels in the band gap [29], contributions from both the A_1 (LO) and E_1 (LO) modes due to random crystallite orientation [29] or a combination of electric field induced (EFI) Raman enhancement and one of the following mechanisms (i) coupled phonon-plasmon scattering or (ii) localised interface and/or surface phonon modes [30].

The absence of the characteristic 2nd, 3rd order scattering in our spectra rules out the resonant enhancement by levels in the gap. These are observed in the spectra of the samples under UV excitation as expected. Contributions from both the A_1 (LO) and E_1 (LO) modes due to random crystallite orientation can also be ruled out for the reasons given by Exarhos and Sharma [29], namely that, after annealing the XRD results remain essentially the same, except for a reduction in the FWHM of the peaks, with no evidence for substantial crystallite reorientation. In addition this cannot explain the abnormally high intensity of the 570 cm^{-1} band in samples (i) and (ii) in particular. Phonon-plasmon coupling is known to produce significant line shifts and broadening in Raman spectra. However, for highly nanocrystalline

material, the contribution of the lower frequency L^- mode is generally absent, and a shift and broadening to higher energy of the L^+ mode is observed. This behaviour is not seen in our samples, hence we believe that the line broadening we observe is unlikely to be due to phonon-plasmon coupling.

The most consistent explanation of the behaviour of our Raman data is in terms of EFI enhancement (via charge trapping at grain boundaries) of the 570cm^{-1} feature [30]. This enhancement effect in conjunction with the presence of localised/surface phonon modes, which arise due to the small grain size, accounts for both the intensity and asymmetry of the peak in the unannealed sample [30]. Surface phonon modes have been reported at ~550cm^{-1} in ZnO [31], which is close to the low energy side of the broad LO mode. This assignment is supported by the appearance of a high energy surface exciton peak in PL data from the unannealed sample (i), mentioned below. In the annealed samples, the increase in the grain size reduces the grain boundary density and hence the effects of charge trapping at grain boundaries. Consequently the EFI enhancement is substantially reduced, in addition to elimination of the surface/interface modes. The importance of band bending at grain boundaries in nanocrystalline samples and the presence of strong electric fields has also been found in studies of varistor action in ZnO [32] and of the green luminescence mechanism [33]. Similar enhancement and asymmetry effects have also been observed in the Raman scattering of ZnO containing gold colloids [34]. These were attributed to a surface enhancement effect caused by anomalously large electric fields due to the colloid plasmon resonance. Thus, our data appear to support the model proposed in references [30, 34]. This suggests that the enhancement and asymmetry of the 570cm^{-1} Raman feature of nanocrystalline ZnO constitutes a good indicator of the grain size of the material.

The PL data previously shown also supports the conclusions reached concerning the roles of grain boundary electric fields. We note that all PLD-grown samples show BE PL. For the unannealed sample the emission is rather weak. The higher energy peak on the shoulder of the main PL line (figure 6(a)) is likely to be due to surface excitons, reported in [35 – 38], which is expected for samples with small grain sizes and consequently large “surface-like” character of the material as mentioned above. The large surface to volume ratio may in turn account for the lower bandedge PL intensity of sample (i) compared to samples (ii) and (iii), due to surface quenching of the exciton features. For the two annealed samples (figure 6(b,c)), we see a substantial change in the band-edge PL, with a much larger intensity for both annealed samples compared to sample (i). We note the appearance of broad lines below the main PL line at energies of 3.330 eV and 3.255 eV with a separation of ~ 75 meV which corresponds closely to the LO phonon energy of 72 meV [39]. A variety of near bandedge excitonic features are seen in nanostructured material, depending on material quality and the concentrations of other impurities [40-41]. We tentatively attribute these PL features to emission from excitons bound to structural defects [42-43] and an LO phonon replica of this emission. Thus with increased annealing we see a substantial and consistent growth in the contribution of BE emission to the PL. This increase in FE luminescence may be expected due to the reduction of the surface to volume ratio of the nanocrystals and the consequent reduction in the surface quenching of bandedge excitonic emission.

Reflectance data has been widely published for bulk ZnO [44-46], but there are few reports on nanocrystalline material such as the PLD samples we have examined. The reflectance data for the bulk crystal shows similar form to those published earlier [46], with A- and B- exciton features at ~ 3.374 eV and 3.390 eV, respectively. Although reflectance

data on the PLD samples is substantially distorted we see clear resonances in samples (i), (ii) and (iii), at ~ 3.374 eV and 3.390 eV.

We now consider the details of the reflectance from the A-and B- excitons in the PLD samples compared to the bulk sample at 20 K. The excitonic reflectance anomalies are substantially damped compared to the bulk crystal, particularly for the unannealed sample, where the reflectance signatures are extremely weak. These features recover in both the annealed samples. A significant strain exists in all the PLD-grown samples, as previously measured by XRD (see table 1). The c-axis lattice parameters for all the PLD-grown samples are 0.518 nm and the values for all samples were identical within the limits of our experimental accuracy. The samples are under tensile biaxial strain following deposition on the (0001) sapphire substrate with strain values of $e_{zz} = -6 \pm 1 \times 10^{-3}$. We have plotted in figure 13 the variation of the A-, B- and C- transverse exciton energies with tensile biaxial strain using the deformation potential Hamiltonian in [47 - 49] and the fit parameters in these papers, with the small exchange interaction term set to zero. We have superimposed on this the positions of the A- , B- and C excitons from the bulk crystal, at zero strain, and the positions of the A- and B-excitons from the PLD samples, all taken at 20 K. For this analysis we use a commonly accepted empirical procedure to determine the longitudinal exciton positions, while below we support this with a more thorough fitting procedure. The position in energy (from figure 6) of the reflectance minimum is taken as the longitudinal exciton energy [50] and the positions of the B- and C- excitons are corrected by the longitudinal-transverse splittings (~10 meV) [47] to give the transverse exciton position. We note that our estimation of the transverse exciton energies in the PLD samples will have an error of ~ ± 2. 5 meV for the B-exciton and ~ ± 1 meV for the A-exciton due to the rather broad excitonic reflectance anomalies in the PLD samples compared to the bulk. Additionally, we have neglected any possible changes in the longitudinal-transverse splittings in the PLD samples compared to the bulk.

One can immediately note that the bulk crystal exciton energies are well described by the model Hamiltonian and the fit parameters from [47 - 49]. The exciton energies for the PLD samples however are different to those predicted by the model. For the unannealed sample the energy difference for the A-exciton is +9 meV and +25 meV for the B-exciton. This reduces in the annealed samples to +6 meV and +8 meV respectively for the sample annealed at 400 ^{0}C and to +6 meV and +11 meV respectively for the sample annealed at 500 ^{0}C (transverse A-exciton at ~ 3.375 eV and B-exciton at ~ 3.388 eV). We note that these energy shifts cannot be adequately explained on the basis of a quantum confinement (QC) shift, as QC shifts in the weak confinement regime, appropriate for ZnO nanocrystals of the sizes observed in our work, would be at most ~1.3 meV for sample (i), reducing to less than 0.5 meV for samples (ii) & (iii) [51]. Thus these shifts would only be responsible for a very small fraction of the overall observed shift. The energy differences for the two annealed samples are identical within the experimental error, but there is a very substantial reduction compared to the unannealed sample. The energy differences are positive in all cases, indicating that the actual energy positions are higher than those expected purely on the basis of strain effects. Additionally, the energy difference for the B-exciton is in all cases larger than that of the A-exciton.

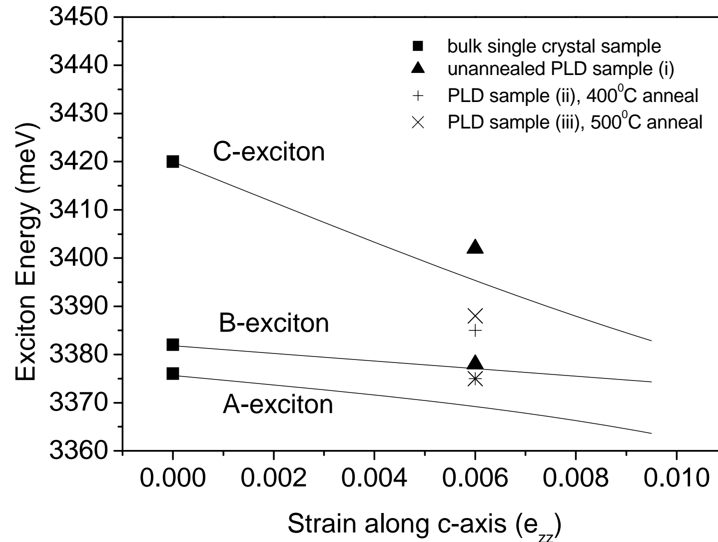

Figure 13: Plot of variation of exciton energy with strain. The continuous lines are the prediction based on the deformation potential model. The other points show the position of the A- and B-excitons for the PLD samples and the bulk sample. For each PLD sample the lower and higher energy data points are the A-exciton and B-exciton transverse energies respectively. The errors in the exciton energy for the PLD samples are ~ 2 meV for the A-exciton and ~5 meV for the B-exciton. The error for the bulk sample is smaller than the data point size.

We conclude that there must be additional perturbing effects on the exciton energies in these samples. As concluded above, x-ray diffraction and Raman spectroscopic measurements on the PLD-grown samples show an oriented, columnar, epitaxial, nanocrystalline grain structure with the grains highly oriented along the c-axis, and a continuous increase in the nanocrystalline grain size with increased annealing. Raman data in particular have shown evidence for electric fields due to depletion layers formed by charge trapping at grain boundaries, which decreased as the grain size increased. We propose that the additional perturbation experienced by the excitons is caused by the same effect. This explains the reduced perturbation observed in the samples annealed at 400 ^{o}C and 500 ^{o}C, as these samples have larger grain sizes (table 1) and hence reduced grain boundary density and electric field effects. The sample annealed at 500 ^{0}C actually has the same A-exciton energy difference as the sample annealed at 400^{0}C, and a slightly larger B-exciton energy difference. However, considering that the grain size in the two annealed samples is quite similar and given the rather large error associated with the transverse energy estimation (particularly for the B-exciton) as mentioned above, we feel that the results are consistent within these error bounds.

Our interpretation of the origin of exciton energy shifts in the PLD samples is in good agreement with theoretical descriptions of the effect of electric fields on exciton energies [52-53]. In reference 52, a universal curve relating the change in exciton energy to the electric field in the sample is given (as a multiple of the ionisation field, corresponding to a potential drop of 1 Rydberg across the exciton Bohr radius, when substantial exciton ionisation begins). For electric fields equal to or greater than the ionisation field the exciton energy difference compared to the zero field case is always positive, in agreement with our data. For

ZnO the exciton energy difference due to such an electric field will have values of the order of ~ 6 meV and greater, again in general agreement with the order of magnitudes in our data.

Visual inspection of the reflectance anomalies shows that there is certainly substantial exciton damping for both A- and B-excitons, which is known to occur for electric fields greater than or equal to the ionisation field [52]. However we can make an independent check of the rough magnitude of the electric field and the ZnO ionisation field as follows. The ionisation field of a wide variety of semiconductors scales linearly with the exciton binding energy [52]. If we extrapolate using the values in reference 52 and the 60 meV binding energy for the exciton in ZnO [1, 43] we find that the ionisation field for ZnO is ~300 x 10^3 V/cm. We may estimate the electric fields in the depletion regions at the grain boundaries using a simple model, similar to that used to determine depletion layer widths in p-n junctions [54]. The residual n-type carrier density in ZnO films grown by PLD on sapphire is generally in the range ≥ 5 x 10^{17} cm^{-3} [23, 55] and the typical potential barriers between grains (of the order of magnitude observed here), associated with these depletion regions, is ≥ 0.1 eV [56]. Hall measurements on our samples show carrier concentrations of ~1 x 10^{19} cm^{-3}. Using these carrier concentrations and the static dielectric constant of ZnO [24, 43, 53], we can estimate that the average electric fields in the depletion layers in our PLD samples will be slightly greater than the ionisation field. Thus we are confident that the electric fields in our samples have values equal to or greater than the ionisation field for the excitons and that the consequent energy perturbations and damping predicted by theory are fully consistent with our data. In addition, this model predicts that a greater energy perturbation is associated with a stronger electric field and consequently greater exciton damping. We have seen that the energy difference for the B-exciton is in all cases larger than that of the A-exciton. Fits to the reflectance data using a polariton model shown below indicate that the B-exciton damping parameter needed to reproduce the data is significantly greater than the A-exciton damping parameter, in agreement with the theoretical predictions above. We also note that the predicted damping parameter, ΔE(F), of absorption spectral lines as a function of electric field, based on WKB theory [57, 58], is given by the equation:

$$\Delta E(F) = (0.35E_B)\exp(\frac{-0.32F_{ion}}{F}) \tag{2}$$

where F is the electric field strength, F_{ion} is the ionisation field, and E_B is the exciton binding energy. Using the parameters given earlier for ZnO, and the estimated field strengths above, we calculate a damping parameter for our samples based on this model of ~15 meV, yielding a good order of magnitude agreement with the values of 6.8 and 13.7 meV calculated from reflectance data for the A- and B-excitons, respectively, as discussed below. This is a good quantitative agreement given the nature of the approximations made.

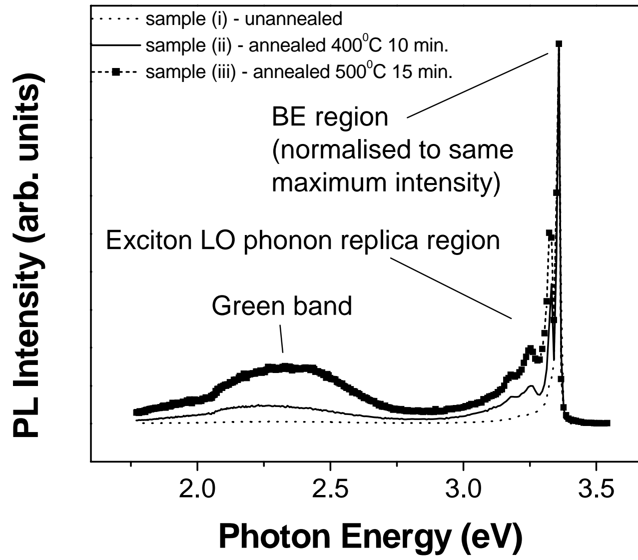

Figure 14: PL data for the three PLD samples at 20 K. The samples are normalised so that the BE peak intensity is the same in all three graphs.

PL data over a wider energy range for the three PLD samples is shown in figure 14. We see a clear trend in the data: the green band intensity increases relative to the BE intensity with increased annealing. The relative strength of the green luminescence in comparison to the band-edge PL is often taken as a measure of the sample quality, with strong green luminescence indicating lower quality. The data presented above indicates a general reduction in defect density with increased annealing, in apparent contradiction with the PL results of figure 14. We can explain these data in a manner consistent with the interpretation above using the model proposed by Vanhuesden et al. [33]. In this model, the green band is attributed to transitions at a singly charged oxygen vacancy (V^{+}_{O}). At grain boundaries, where band-bending effects are substantial due to trapped charges, as mentioned above, these vacancies become doubly ionised (V^{++}_{O}) and the green luminescence is quenched. Our data are consistent with this model as the increase in grain size with annealing causes a reduction in the grain boundary density and hence the fraction of V^{++}_{O} compared to V^{+}_{O}. This results in an increase in the green luminescence band intensity with increasing grain size. This interpretation is also consistent with the results previously obtained by de Posada et al. [59].

In order to describe the reflectance spectra in more detail and to confirm the conclusions based on our empirical determination of the transverse exciton energies, we will use a two band exciton resonance model, with appropriate boundary conditions for a thin film on sapphire or a bulk slab (i.e. semi-infinite) [24]. The transverse modes are found by solving the following equation for k^2:

$$\frac{k^2c^2}{\omega^2} = \varepsilon_\infty + \frac{\alpha_{0A}}{\varepsilon_0}\left(\frac{\omega_{AT}^2}{\omega_{AT}^2 - \omega^2 + \beta_A k^2 - i\omega\Gamma_A}\right) + \frac{\alpha_{0B}}{\varepsilon_0}\left(\frac{\omega_{BT}^2}{\omega_{BT}^2 - \omega^2 + \beta_B k^2 - i\omega\Gamma_B}\right) \quad (3)$$

where the symbols have their customary meaning [24] . These solutions are used with suitable EM boundary conditions and ABC's to calculate the reflectance spectra. We have chosen to use the Pekar ABCs, with the excitonic polarisation vanishing for each band, at each interface. For the bulk sample we also use an exciton dead-layer of variable thickness in the fit [60]. In figure 8(a) we show the best fit to the bulk crystal experimental data of figure 8(b). The reflectance anomalies are well described by the fit. The fit parameters are given in table 2 and are similar to those found in Ref. [24]. To fit the reflectance data for the PLD samples firstly we began by fitting the excitonic region (region II) neglecting the thin film nature of the sample for the sample annealed at 500^0C. To date we have not fitted the reflectance data for all other the PLD-grown samples. Our fitting of the sample annealed at 500^0C is mainly to corroborate the conclusions drawn earlier on the basis of the empirical determination of longitudinal and transverse exciton energies and to explain the general features seen in the reflectance data.

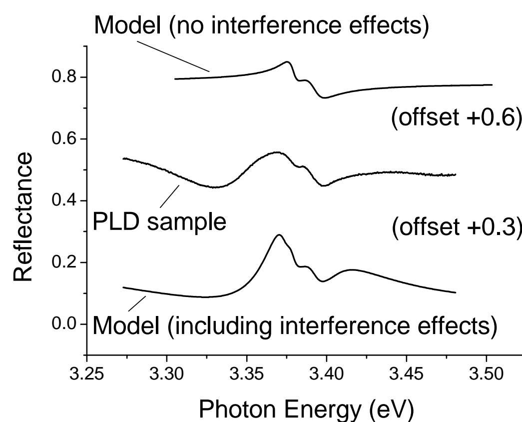

Figure 15: Comparison of the reflectance spectra of the PLD sample annealed at 500^0C (middle curve) with computed reflectance spectra; without including thin film interference effects (top curve); including thin film interference effects (bottom curve).

This fit is shown in figure 15(a), and it may be seen that region II of the experimental curve (figure 15(b)) is well described by this fit, with the parameters given in table 2. One may compare the parameters for the PLD sample with those found for the bulk sample in table 2. There is a substantial shift in the positions of the A- and B-excitons and also a change in the transverse A-B splitting, due to both biaxial strain arising from lattice mismatch with the substrate and grain boundary electric fields. The LT splitting of the B-exciton in the PLD sample is also substantially different to the value in the bulk crystal. The physical origin of such a dramatic difference is not clear, but may also be due to the combination of strain and electric fields in these samples. In particular, we note that the transverse A- and B-exciton energies determined by this fit for this sample are ~ 3.378 eV and ~ 3.390 eV respectively, compared to values of 3.375 eV and 3.388 eV from our empirical determination earlier. The agreement is reasonably good, and the fitted values are in both cases slightly higher than the empirically determined ones, thus providing even grater support for the presence of additional perturbations on the exciton energies in addition to strain. It is also clearly seen that the exciton damping factors for the A- and B-excitons in the PLD sample are much larger than

the values in the bulk sample as expected on the basis of the significantly poorer crystal quality of the PLD material and the small grain sizes, and, again in agreement with our observations earlier, the damping factor of the B-exciton is approximately twice that of the A-exciton. The exciton "dead-layer" thickness in the fit for the PLD sample is zero, while the exciton effective mass is 0.5 times the electron mass. While both these values are different to those found for the bulk sample, the fit is largely insensitive to these parameters given the rather large damping. Visually identical spectra are computed with the bulk values of these quantities. The oscillations in regions I and III are not reproduced by this fit (figures 15(a) and (b)). We have thus used a multi-layer model of an air-ZnO-sapphire (refractive index of sapphire ~ 1.8) structure, using identical parameters to those found in fitting the excitonic region, with the ZnO film thickness as an additional variable. Fitting this model to the data we get the curve in Fig. 15(c), with a ZnO layer thickness of 215 nm, in good agreement with the known values of film thickness. The agreement between the experimental data in Fig. 15(b) and the fit in Fig. 15(c) is qualititatively good. The reflectance minimum at ~ 3.327 eV and the reflectance increase at lower energies are reproduced as is the oscillatory behaviour in the 3.4 – 3.45 eV range. The origin of this behaviour, where FP oscillations are seen at energies below and above the exciton-photon interaction region, while the central excitonic region is well described by a model neglecting the thin film nature of the sample, may be understood as follows. Figure 16 shows the dispersion of the exciton-polaritons in ZnO and indicates regions I, II and III, as in figures 7 and 8. FP oscillations will only be observed if the spatial damping of the propagating modes is sufficiently small that the modes can make at least two passes through the film. This condition is quantified by requiring that the sample thickness d is significantly less than L, where $L = (n_i.k_o)^{-1}$, n_i is the imaginary part of the mode refractive index and k_o the free space wavevector [61]. The L values of the photon-like branches in regions I and III, where mixing with the highly damped exciton is minimal, are ~ 120,000 nm and ~ 40,000 nm respectively and L >> 200 nm. Thus we expect to see oscillatory structure in the reflectance. In region II L for all modes is < 400 nm due to the large damping of the exciton and the strong exciton-photon mixing. Thus no oscillations would be expected in region II, in agreement with observation [62-63].

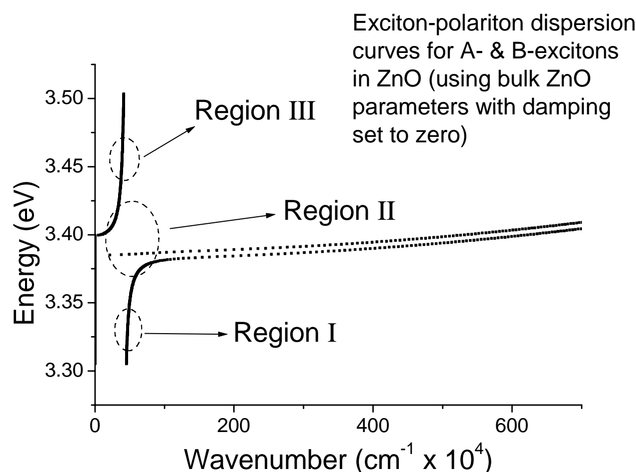

Figure 16: Dispersion of the exciton-polaritons associated with the A- & B-excitons in ZnO (bulk ZnO parameters used with damping set to zero).

Table 2: Fit parameters for bulk & PLD samples using two band exciton model. Final column gives literature values for ZnO single crystal.

Parameter	Bulk crystal	PLD sample (sample (iii) annealed at 500^{0}C)	Literature value [24]
$\hbar\varpi_{AT}$ (transverse A exciton energy, eV)	3.3753	3.3781	3.3758
$\hbar\varpi_{BT}$ (transverse B exciton energy, eV)	3.3813	3.3904	3.3810
$\hbar\varpi_{AT}$ - $\hbar\varpi_{BT}$ (A-B splitting, meV)	6	12.3	5.2
Δ_{LT}^{A} (A exciton LT splitting, meV)	2	1.9	1.8
Δ_{LT}^{B} (B exciton LT splitting, meV)	11.9	3.6	10.2
$\hbar\Gamma_{A}$ (A exciton damping, meV)	0.7	6.8	0.7
$\hbar\Gamma_{B}$ (B exciton damping, meV)	0.7	13.7	0.7
M (multiples of electron mass)	0.87	0.5	0.87
Dead-layer thickness (nm)	4	0	4

Turning to the high excitation data described previously, perhaps the most interesting point is that while high excitation effects and even lasing are seen in the PLD samples at room temperature, no evidence of such effects is seen in bulk material of obviously superior optical quality, as evidenced by PL and reflectance. Other authors have noted that poly- or nanocrystalline thin films, unlike bulk ZnO material, exhibit low thresholds for the appearance of non-linear emission bands and optically pumped stimulated emission [64-67]. The origin of this behaviour compared to bulk material has been attributed to giant excitonic oscillator strengths in low dimensional nanocrystalline structures, based on theoretical studies [64, 68]. Quite clearly, as indicated earlier, our PLD samples have substantially inferior optical quality compared to bulk material, and, in particular, the value of the longitudinal-transverse splitting for the A- and B- excitons is smaller in the PLD samples than in the bulk material (table 2). It is also worth noting that other linear optical measurements reported in the literature (e.g. PL, absorption and reflectance) on poly- or nanocrystalline ZnO which show lasing at room temperature also reveal no evidence of giant oscillator strengths [64-67, 28], similar to our data. Various authors have suggested that the wave-guiding properties of the air / ZnO / sapphire structure affects the stimulated emission properties leading to large gains in thin films [69]. The critical film thicknesses identified are ~ 50 – 60 nm, substantially thinner than our films. Hence we do not believe that this effect is appropriate to explain our data either. An alternative and simpler explanation is that the FE density in nanocrystalline materials may be substantially higher than that in bulk material under the same conditions of above bandgap excitation, due to inhibition of FE diffusion in nanocrystalline samples at grain boundaries, similar to effects seen in thin films [70-71]. The P- and electron-hole pair (EHP) bands in which stimulated emission and lasing are normally seen grow proportional to the second (or higher) powers of the FE density [26] and are thus very sensitive to the exciton density. In nanocrystalline samples the FE population created by optical pumping in the ~ 50nm penetration depth [72] will be strongly confined in this volume by grain boundaries [65]. In contrast, FE diffusion lengths in bulk material may be significantly larger. FE diffusion lengths at low temperature (<77K) are reported in the range 0.2 – 2 μm [70, 72-74],

and hence the initial exciton population will diffuse and lower its density substantially. This explanation is outlined in more detail in reference 75, where it is shown that changes in the superlinear optical emission bands (P-band, EHP) may be 2 – 3 orders of magnitude larger in nanocrystalline ZnO (with grain sizes ~50 nm) compared to bulk material [75].

An inter-comparison of the high excitation data from the three PLD samples is consistent with the data presented from other optical techniques, and shows that the annealed samples, particularly sample (iii) shows the best optical quality, and in this case is the only sample to show random lasing behaviour [76].

Conclusion

Pulsed laser deposited ZnO thin films have been characterized using XRD, AFM, Raman spectroscopy, PL (at high and low excitation) and reflectance spectroscopies. All films show dominant c-axis orientation with epitaxial in-plane ordering. The evolution of the FWHM of the XRD (0002) peaks with annealing temperature indicates an increase in the nanocrystalline grain size which is confirmed by AFM measurements. A strong correlation between the enhancement and asymmetry of the 570cm^{-1} Raman mode and the FWHM of the XRD data has been observed. The presence of electric fields, due to charge trapping at grain boundaries, in addition to localised and surface phonon modes, explains the intensity enhancement and asymmetry of the LO mode in the unannealed sample. An increase in the grain size and reduction in the electric field intensity due to annealing lead to a decrease in the intensity and asymmetry of the LO mode.

Our PL and reflectance measurements show a consistent increase of material quality, in terms of PL band-edge emission intensity, linewidth and excitonic reflectance features, with increased annealing, though they still fall far short of the bulk crystal material, with excitonic linewidths approximately an order of magnitude larger. The PL spectra of the material show an increase in bandedge BE signal with increased annealing. The reflectance data show similar trends, and assignments are made for the A- and B-exciton features on the reflectance spectra. Substantial shifts and quenching of the A- and B-excitons are observed and these support the previous conclusions concerning the importance of electric field effects in these samples. We also see a consistent increase in the intensity of the green luminescence band with increased annealing and explain this in terms of a previously reported model based on oxygen vacancies ionised due to electric fields, consistent with the interpretation of our band-edge data.

A model based on the interaction of strongly damped excitons with a photon mode adequately describes the experimental data and this model supports the conclusions drawn from an empirical determination of the exciton parameters. FP oscillations are observed both above and below the strong interaction regime, where the photon-like mode is weakly damped. In the strong interaction regime, where all propagating modes are strongly damped due to mixing, no oscillations are seen. Thus we find that it is important to consider the full polariton picture in interpreting the reflectance spectra of nanocrystalline ZnO material.

We observe evidence of high excitation effects in all PLD samples, but evidence of lasing only in the sample (iii) annealed at 500^{0}C. The P-band was identified in each of the PLD samples but became most obvious in this sample. The variation in the strength of the P-band and the onset of lasing was again consistent with the optical properties of the PLD samples

observed via the other experimental techniques. The presence of such nonlinear optical emission bands in nanocrystalline PLD thin films compared to superior optical quality bulk material is attributed to the inhibition of exciton diffusion in nanocrystalline films, leading to a large enhancement in the exciton density compared to bulk material.

Acknowledgements

The authors wish to acknowledge financial support provided by the Enterprise Ireland Basic Research Grants programme, the Science Foundation Ireland Principal Investigator Grants programme (under grant number 02/IN1/I95) and the financial support of the Higher Education Authority through the PRTLI programme. We also gratefully acknowledge the assistance of Dr. Jean-Rene Duclère in making and interpreting the XRD phi-scan measurements.

We note with deep sadness the death of our colleague, Dr. Chaitali Roy. Chaitali passed away in the period between the initial preparation of this work and its final publication, following a long illness which she bore with characteristic patience, courage and dignity. Chaitali made a number of very important contributions to our understanding of the effects which electric fields have on the Raman spectra measured on PLD-grown samples, which in turn formed the basis of our broader understanding of the optical properties of these samples.

References

[1] Look, D.C. *Mat. Sci. & Eng. B* 2001, 80, 383-387.
[2] Chen, Y.; Bagnall, D.; Yao, T. *Mat. Sci. & Eng. B* 2000, 75, 190-198.
[3] Look, D.C.; Reynolds, D.C.; Fang, Z.-Q.; Hemsky, J.W.; Sizelove, J.R.; Jones, R.L. *Mat. Sci. & Eng. B* 2000, 66, 30-32.
[4] Ryu, Y.R.; Zhu, S.; Look, D.C.; Wrobel, J.M.; Jeong, H.M.; White H.W. *J. Crystal Growth* 2000, 216, 330-334.
[5] Tsukazaki, A.; Ohtomo, A.; Onuma, T.; Ohtani, M.; Makino, T.; Sumiya, M.; Ohtani, K.; Chichibu, S. F.; Fuke, S.; Segawa, Y.; Ohno, H.; Koinuma H.; Kawasaki, M. *Nature Materials* 2005, 4, 42- 46.
[6] Ip, K.; Heo, Y. W.; Norton, D. P.; Pearton, S. J.; LaRoche, J. R.; Ren, F. *Appl. Phys. Lett.* 2004, 85, 1169-1171.
[7] Huang, M.H.; Mao, S.; Feick, H.; Yan, H.; Wu, Y.; Kind, H.; Weber, E.; Russo, R.; Yang, P. *Science* 2001, 292, 1897-1899.
[8] Wang, Z.L. J. Phys.: *Condens. Matter* 2004, 16, R829-R858.
[9] Zhang, B.P.; Binh, N.T.; Wakatsuki, K.; Segawa, Y.; Kashiwaba, Y.; Haga, K. *Nanotechnology* 2004, 15, S382-S388.
[10] Heiland, G.; Mollwo, E.; Stockmann F. *Solid State Phys.*1959, 8, 191-323.
[11] Muth, J.F.; Kolbas, R.M; Sharma, A.K; Oktyabrsky, S.; Narayan, J. *J. Appl. Phys.* 1999, 85, 7884-7887.
[12] Makino, T.; Yasuda, T.; Segawa, Y.; Ohtomo, A.; Tamura, K.; Kawasaki, M.; Koinuma, H. *Appl. Phys. Lett.* 2001, 79, 1282-1284.

[13] Krishnamoorthy, S.; Iliadis, A.A.; Inumpudi, A.; Choopun, S.; Vispute, R.D.; Venkatesan, T. *Solid State Electronics* 2002, 46, 1633-1637.
[14] Lorenz, M.; Hochmuth, H.; Schmidt-Grund, R.; Kaidashev, E.M.; Grundmann, M. *Ann. Phys*. (Leipzig) 2004, 13, 59-60.
[15] Oshima, T.; Thareja, R.K.; Yamagata, Y.; Ikegami, T.; Ebihara, K.; Narayan*, J. Sci.Tech. Adv. Mat.* 2001, 2, 517-523.
[16] Cullity, B.D. *Elements of X-ray Diffraction*; Addison-Wesley: London, 2nd ed. 1978; pp 99-103.
[17] Bae, S.H.; Lee, S.Y.; Kim, H.Y.; Im, S. *Opt. Mater*. 2001, 17, 327-330.
[18] Gupta, V.; Mansingh, A. *J. Appl. Physics* 1996, 80, 1063-1073.
[19] Puchert, M. K.; Timbrell, P. Y.; Lamb, R. N. *J. Vac. Sci. Technol. A* 1996, 14, 2220-2230.
[20] Arguello, C.A.; Rousseau, D.L.; Porto, *S.P.S. Phys. Rev*. 1969, 181, 1351-1363.
[21] Zhang, X.T.; Liu, Y.C.; Zhi, Z.Z.; Zhang, J.Y.; Lu, Y.M.; Shen, D.Z.; Xu, W.; Zhong, G.Z.; Fan, X.W.; Kong, X.G. *J. Phys. D: Appl. Phys*. 2001, 34, 3430-3433.
[22] Scott, J.F. *Phys. Rev. B* 1970, 2, 1209-1211.
[23] Jin, B.J.; Im, S.; Lee, S.Y. *Thin Solid Films* 2000, 366, 107-110.
[24] Lagois, *J. Phys. Rev. B* 1981, 23, 5511-5520;
[25] Lagois, *J. Phys. Rev. B* 1977, 16, 1699-1705.
[26] Klingshirn , C. Phys. *Status Solidi B* 1975, 71, 547-556.
[27] Bagnall, D.M.; Chen, Y.F.; Zhu, Z.; Yao, T.; Koyama, S.; Shen, M.Y.; Goto, T. *Appl. Phys. Lett* 1997, 70, 2230-2232.
[28] Bagnall, D.M.; Chen, Y.F.; Shen, M.Y.; Zhu, Z.; Goto, T.; Yao, T. *J. Crys. Growth* 1998, 184/185, 605-609.
[29] Exarhos, G.J.; Sharma, S.K. *Thin Solid Films* 1995, 270, 27-32.
[30] Tzolov, M.; Tzenov, N.; Dimova-Malinovska, D.; Kalitzova, M.; Pizzuto, C.; Vitali, G.; Zollo, G.; Ivanov, I. *Thin Solid Films* 2000, 379, 28-36.
[31] Ibach, H. *Phys. Rev. Lett*. 1970, 24, 1416-1418.
[32] Mahan, G.D. *J. Appl. Phys*. 1983, 54, 3825-3832.
[33] Vanheusden, K.; Warren, W.L.; Seager, C.H.; Tallant, D.R.; Voight, J.A.; Gnade, B.E. *J. Appl. Phys.* 1996, 79, 7983-7990.
[34] Bozlee, B.J.; Exarhos, G.J. *Thin Solid Films* 2000, 377-378, 1-7.
[35] Roy, C.; Byrne, S.; McGlynn, E.; Mosnier, J-P; dePosada, E.; O'Mahony, D.; Lunney, J. G.; Henry, M.O.; Ryan, B.; Cafolla, A.A. *Thin Solid Films* 2003, 436, 273-276.
[36] Savikhin, S.; Freiberg, A. *J. Lumin*. 1993, 55, 1-3.
[37] Travnikov, V.V., Freiberg, A.; Savikhin, S. *J. Lumin*. 1990, 47, 107-112.
[38] Grabowska, J.; Meaney, A.; Nanda, K.K.; Mosnier, J.-P.; Henry, M.O.; Duclère, J.-R.; McGlynn E. *Phys. Rev. B* 2005, 71, article #115439.
[39] Tobin, G.; Fryar, J.; McGlynn, E.; Mosnier, J-P.; Henry, M.O.; dePosada, E.; O'Mahony, D.; Lunney J.G. In Physics of Semiconductors 2002; Long, A.R.; Davies, J.H.; Ed.; Institute of Physics Conference Series Number 171: IOPP, Bristol, 2002; paper number H26.
[40] Weiher, R.L.; Tait, W.C. *Phys. Rev*. 1968, 166, 791-796.
[41] Zhang, B.P.; Binh, N.T.; Segawa, Y.; Kashiwaba, Y.; Haga, K. *Appl. Phys. Lett*. 2004, 84, 586-588.

[42] Schildknecht, A.; Sauer, R.; Thonke, K. *Physica B* 2003, 340-342, 205-209.

[43] Meyer, B.K.; Alves, H.; Hofmann, D.M.; Kriegseis, W.; Forster, D.; Bertram, F.; Christen, J.; Hoffmann, A.; Strassburg, M.; Dworzak, M.; Haboeck, U.; Rodina, A.V. *Phys. Stat. Solidi (b)* 2004, 241, 231-260.

[44] Zhang, B.P.; Binh, N.T.; Segawa, Y.; Wakatsuki, K.; Usami, N. *Appl. Phys. Lett*. 2003, 83, 1635-1637.

[45] Ozaki, S.; Mishima, T.; Adachi, S. *Jpn. J. Appl. Phys*. 2003, 42, 5465-5471.

[46] Reynolds, D.C.; Look, D.C.; Jogai, B.; Jones, R.L.; Litton, C.W.; Harsch, W.; Cantwell, G. *J. Lumin*. 1999, 82, 173-176.

[47] McGlynn, E.; Fryar, J.; Tobin, G.; Roy, C.; Henry, M.O.; Mosnier, J.-P.; dePosada, E.; Lunney, J.G. *Thin Solid Films* 2004, 458, 330-335.

[48] Gil, B.; Lusson, A.; Sallet, V.; Daid-Hassani, S.; Triboulet, R.; Bigenwald, P. Jpn. *J. Appl. Phys*. 2001, 40, L1089-L1092.

[49] Wrzesinski, J.; Frohlich, D.; *Phys. Rev. B* 1997, 56, 13087-13093.

[50] Hopfield, J.J.; Thomas, D.G. Phys. *Rev. Lett*. 1965, 15, 22-25.

[51] Basu, P.K. *Theory of Optical Processes in Semiconductors*; Oxford Science Publications: Oxford, 1997; pp 358-359.

[52] Blossey, D.F.; *Phys. Rev. B* 1971, 3, 1382-1391.

[53] Taken from data in Landolt-Bornstein, *Numerical Data and Functional Relationships in Science and Technology*; Rossler, U.; Ed.; New Series III; Springer: Berlin, 1999; Vol. 41B, on CD.

[54] Yang, E.S. *Fundamentals of Semiconductor Devices*; McGraw-Hill: New York, NY, 1978; pp 85-89.

[55] Ohtomo, A.; Tamura, K.; Saikusa, K.; Takahashi, K.; Makino, T.; Segawa, Y.; Koinuma, H.; Kawasaki, M. *Appl. Phys. Lett.* 1999, 75, 2635-2637.

[56] Srikant, V.; Clarke, D.R. *J. Appl. Phys*. 1997, 81, 6357-6364.

[57] Ralph, H.I. *J. Phys. C* 1968, 1, 378-386.

[58] Schultheis, L.; Lagois, *J. Phys. Rev. B* 1984, 29, 6784-6790.

[59] dePosada, E.; Tobin, G.; McGlynn, E.; Lunney, J.G. *Appl. Surf. Sci*., 2003, 208-209, 589-593.

[60] Hopfield, J.J.; Thomas, D.G. *Phys. Rev.* 1963, 132, 563-572.

[61] Ivchenko, E.L. In Excitons; Rashba, E.I.; Sturge, M.D.; Ed.; North-Holland: Amsterdam; 1982; pp 141-176.

[62] McGlynn, E.; Fryar, J.; Henry, M.O.; Mosnier, J.-P.; Lunney, J.G.; O'Mahony, D.; DePosada, E. *Physica B* 2004, 458, 230-234.

[63] Fryar, J.; McGlynn, E.; Henry, M.O.; Mosnier, J.-P. *Nanotechnology* 2005 16, 2625-2632.

[64] Zu, P.; Tang, Z.K.; Wong, G.K.L.; Kawasaki, M.; Ohtomo, A.; Koinuma, H.; Segawa, Y. *Solid State Commun.* 1997, 103, 459-463.

[65] Kawasaki, M.; Ohtomo, A.; Ohkubo, I.; Koinuma, H.; Tang, Z.K.; Yu, P.; Wong, G.K.L.; Zhang, B.P.; Segawa, Y. *Mat. Sci. and Eng. B* 1998, 56, 239-245.

[66] Zhang, X.Q.; Suemune, I.; Kumano, H.; Wang, J.; Huang, S.H.; *J. Appl. Phys.* 2004, 96, 3733-3736.

[67] Zhi-Gang, Y.; Xi-Qing, Z.; Hong-Kai, S.; Xiao-Ying, T.; Yong-Sheng, W.; Shi-Hua, H. *Chinese Physics* 2005, 14, 1205-1208.

[68] Kayanuma, Y. *Phys. Rev. B* 1988, 38, 9797-9805.
[69] Yu, P.; Tang, Z.K.; Wong, G.K.L.; Kawasaki, M.; Ohtomo, A.; Koinuma, H.; Segawa, Y. *J. Crys. Growth* 1998, 184-185, 601-604.
[70] Klingshirn, C. *Semiconductor Optics*, 2nd ed. Springer: Berlin, 2005.
[71] Priller, H.; Brückner, J.; Gruber, Th.; Klingshirn, C.; Kalt, H.; Waag, A.; Ko, H.J.; Yao, T. *Phys. Stat. Sol. (b)* 2004, 241, 587-590.
[72] Liang, W.Y.; Yoffe, A.D. *Phys. Rev. Lett.* 1968, 20, 59-62.
[73] Weiher, R.L.; Tait, W.C. *Phys. Rev. B* 1972, 5, 623-627.
[74] Hvam, J. M. *Phys. Stat. Solidi (b)* 1974, 63, 511-517.
[75] Tobin, G.; McGlynn, E.; Henry, M.O.; Mosnier, J.-P.; dePosada, E.; Lunney, J.G. *Applied Physics Letters* 2006, 88, article # 071919.
[76] Tobin, G.; McGlynn, E.; Henry, M.O.; Mosnier, J.-P.; Lunney, J.G.; O'Mahony, D.; DePosada, E. *Physica B* 2004, 458, 245-249.